ISSN 0915-633X

NATIONAL INSTITUTE FOR FUSION SCIENCE

Contributions to the 8th IAEA Technical Committee Meeting on
H-Mode Physics and Transport Barriers
(5-7 September 2001, Toki, Japan)

S. Toda, M. Kawasaki, N. Kasuya, K. Itoh, Y. Takase,
A. Furuya, M. Yagi and S. -I. Itoh

(Received - Sep. 11, 2001)

NIFS-714 Oct. 2001

RESEARCH REPORT
NIFS Series

TOKI, JAPAN

Contributions to the 8th IAEA Technical Committee Meeting on H-Mode Physics and Transport Barriers (5-7 September 2001, Toki, Japan) by S. Toda *et al.*

S. Toda, M. Kawasaki, N. Kasuya, K. Itoh, Y. Takase, A. Furuya, M. Yagi and S. –I. Itoh

Abstract
Three papers have been presented at the 8th IAEA technical committee Meeting on H-Mode Physics and Transport Barriers (5-7 September 2001, Toki, Japan) by above authors (S. Toda *et al.*) as theoretical works. The contributed papers are collected in this report.

F14 S. Toda and K. Itoh, "Theoretical study of transition of radial electric field in helical plasmas"

F08 M. Kawasaki, A. Furuya, M. Yagi, K. Itoh and S. –I. Itoh, "Transition Probability to Turbulent Transport Regime and Its Critical Exponent"

C09 N. Kasuya, K. Itoh and Y. Takase, "Multiple bifurcation of the radial electric field structure induced by electrodes in tokamaks"

Keywords: theoretical works, 8th IAEA Technical Committee Meeting on H-Mode Physics and Transport Barriers, contributed papers

Theoretical study of transition of electric field in helical plasmas

S. Toda and K. Itoh

National Institute for Fusion Science, Oroshi-cho 322-6, Toki 509-5292, Japan

E-mail: toda@ms.nifs.ac.jp

Abstract. A set of transport equations is analyzed, including the bifurcation of the electric field. The structure of the electric field is studied by use of the theoretical model for the anomalous transport diffusivities. Multiple solutions of E_r for the ambipolar condition are examined in the structure of the radial electric field. Parameter region in which the multiple solutions of electric field exist is studied in the case by use of the device parameter of Compact Helical System (CHS). A spatial structure of the radial electric field is also examined in the case using the device parameter of Large Helical Device (LHD).

PACS numbers: 52.25.Fi,52.35.Ra,52.55.-s,52.55.Dy,52.55.Hc

Submitted to: *Plasma Phys. Control. Fusion*

1. Introduction

The internal transport barrier has been found in electron cyclotron resonance heating (ECRH) plasma in CHS and the steep gradient in the profile of the radial electric field has been obtained in the inner region [1]. There are two important issues. The first is the formation of the electric-field domain interface, which is associated with the steep gradient of the radial electric field E_r. The generation of the electric field in helical systems could be investigated more quantitatively because the neoclassical transport is found to play the dominant role in generating the radial electric field (See reviews, *e.g.*, [2, 3]). Study on the localized structure of the gradient of E_r has been performed. [4] The second is the study of the turbulent transport and the neoclassical energy transport so as to understand the formation of the internal transport barrier. The self-consistent transport study has been done in which both the electric field bifurcation and suppression of the anomalous transport are included in order to analyze the structure of the electric field quantitatively [5]. The transport model (e.g. [6]) for anomalous diffusivities was adopted in CHS typical machine parameters.

In this article, types of the structure of the radial electric field is studied and a phase diagram of a bifurcation of E_r profile is investigated. In addition, the transport analysis is extended to simulate an LHD plasma. The E_r structure is examined in the both cases by use of the CHS and LHD machine parameters. The parameter region with respect to the density and the temperature is shown to obtain the electron root ($E_r > 0$).

2. One-dimensional Model Equations

The cylindrical coordinate is used and r-axis is taken in the radial cylindrical plasma in this article. The region $0 \leq r \leq a$ is considered, where a is the minor radius. The total particle flux Γ^t is written as $\Gamma^t = \Gamma^{na} - D_a n'$, where D_a is the anomalous particle diffusivity and the prime denotes the derivative with respect to the radial direction. Here, Γ^{na} is the radial neoclassical flux associated with helical-ripple trapped particle [7]. The total heat flux Q_j^t of the species j is written as $Q_j^t = Q_j^{na} - n\chi_a T_j'$, where χ_a is the anomalous heat diffusivity and Q_j^{na} is the energy flux by the ripple transport, respectively. The theoretical model for the anomalous heat conductivity will be explained later. The neoclassical diffusion coefficient for the electric field is shown in ref. [8] and is denoted by D_{Ea}. The one-dimensional transport equations used here are same as those shown in ref. [4].

3. Boundary conditions and the model of anomalous transport coefficients

We fix the boundary condition at the center of the plasma (r=0) such that $n' = T_e' = T_i' = E_r = 0$. For the radial electric field E_r, the boundary condition at the edge (r=a) is chosen as $\sum_j Z_j \Gamma_j = 0$. This simplification is employed because the electric

field bifurcation in the core plasma is the main subject of this study. The boundary conditions at the edge (r=a) with respect to the density are those expected in the CHS and the LHD: $-n/n' = 0.05(m)$, $-T_e/T_e' = -T_i/T_i' = 0.02(m)$. The machine parameters are similar to those of CHS device, such as $R = 1\mathrm{m}$, $a = 0.2\mathrm{m}$, the toroidal magnetic field $B = 1\mathrm{T}$, toroidal mode number $m = 8$ and the poloidal mode number $\ell = 2$. We set the safety factor and the helical ripple coefficient as $q = 3.3 - 3.8(r/a)^2 + 1.5(r/a)^4$ and $\varepsilon_h = 0\ 231(r/a)^2 + 0.00231(r/a)^4$, respectively [1]. On the other hand, the machine parameters which are similar to those of LHD device are set to be $R = 3.6\mathrm{m}$, $a = 0.6\mathrm{m}$, $B = 3\mathrm{T}$, $m = 10$ and $\ell = 2$. In this case, we set the safety factor and the helical ripple coefficient as $q = 1/(0.4+1.2(r/a)^2)$ and $\varepsilon_h = 2\sqrt{1-(2/(mq(0))-1)^2)}I_2(mr/R)$, respectively. Here, $q(0)$ is the value of the safety factor at $r = 0$ and I_2 is the second order modified Bessel function. The particle source S_n is set to be $S_n = S_0 \exp((r-a)/L_0)$, where L_0 is set to be $0.01(m)$ and the value of S_0 is strongly influenced by the particle confinement time. The value for the anomalous diffusivities of the particle is chosen $D_a = 10\mathrm{m}^2\mathrm{s}^{-1}$. This value is set to be constant spatially and temporally.

In this study, we adopt the model for the anomalous heat conductivity based on the theory of the self-sustained turbulence due to the ballooning mode and the interchange mode, both driven by the current difffusivity [6, 9]. The reduction of the anomalous transport due to the inhomogeneous radial electric field was theoretically reported in the toroidal helical system. (The validity of this model for heliotron/torsatron plasmas has not completely been investigated. This model predicted a trend of χ_a that χ_a can reduce as the magnetic axis is shifted inward. This has some relevance for the experimental observation [10]. The anomalous transport coefficient for the temperatures is given as $\chi_a = \chi_0/(1 + G\omega_{E1}^2)$, where $\chi_0 = F(s,\alpha)\alpha^{\frac{3}{2}}c^2 v_A/(\omega_{pe}^2 qR)$. The factor $F(s,\alpha)$ is the function of the magnetic shear s and the normalized pressure gradient α, defined by $s = rq'/q$ and $\alpha = -q^2 R\beta'$. For the ballooning mode turbulence for the system with a magnetic well, we employ the anomalous thermal conductivity $\chi_{a,BM}$. The details about the coefficients $F(s,\alpha)$, G, and the factor ω_{E_1}, which stands for the effect of the electric field shear, are given in ref. [9] in the balloonig mode turbulence. In the case of the interchange mode turbulence for the system of the magnetic hill [6], we adopt the the anomalous thermal conductivity $\chi_{a,IM}$. The details about F, G, and the factor ω_{E_1} in the case of the interchange mode were given in ref. [6]. The greater one of the two diffusivities is adopted, $\chi_a = \max(\chi_{a,BM}, \chi_{a,IM})$. The approximation $D_{Ea} = \chi_a$ is employed, where the validity of this approximation is discussed in ref. [11].

4. Results of analysis

4.1. Solutions by use of machine parameters of CHS

At first, we use the machine parameters of CHS. In order to set the line-averaged temperature of electrons to be around $\bar{T}_e = 250\mathrm{eV}$ (T_e at the center, $T_e(0) = 900\mathrm{eV}$) and the line-averaged density to be around $\bar{n} = 1 \times 10^{19}\mathrm{m}^{-3}$, the absorbed power of

electrons is 100kW and the coefficient S_0 is $7 \times 10^{24}\mathrm{m}^{-3}\mathrm{s}^{-1}$ for the choice of above values of the anomalous transport coefficients. The line-averaged ion temperature $\bar{T}_i$ is chosen to be about $\bar{T}_i = 150\mathrm{eV}$ (T_i at the center, $T_i(0) = 500\mathrm{eV}$), where the absorbed power of ions is fixed at 50kW.

The stationary solutions of the radial electric field are shown in figure 1(a). At the point ($\rho = \rho_T(0.6)$), the transition of the radial electric field is found. The circles in figure 1(a) show the values of the electric field which satisfy the local ambipolar condition for the calculated profiles of the density and the temperatures. Multiple solutions exist for the local ambipolar condition in the parameter region examined here. We call the hard transition when the transition occurs between the multiple solutions for the local ambipolar condition. In the case of figure 1(a), the electron root for $\rho < \rho_T$ is sharply connected to the ion root for $\rho > \rho_T$ with a thin layer between them. The absolute value of the gradient for the electric field at the transition point $\rho = \rho_T$ is about $1.6 \times 10^6\mathrm{V/m}^2$. The transport barrier is obtained for the both channels of the sum of the neoclassical transport and the anomalous transport, although it is not very clear in both the electron and ion temperature profiles. In figure 1(b), the reduction of χ_a is obtained due to the strong gradient of the electric field at the transition point. The neoclassical diffusivities of electrons χ_e^{NEO} and ions χ_i^{NEO} are also shown with the dashed line and the dotted line, respectively. In the case of the spatial transition in figure 1(a), the electric field goes across zero at $\rho \approx \rho_T$. Therefore, the neoclassical diffusivities have a peak near the surface where the relation $E_r \approx 0$, because they depend on the value of E_r itself. The total suppression is found to exist but is small compared with that of the anomalous diffusivity.

4.2. Phase diagram of the bifurcation of the E_r structure

When the value of the temperature or the density changes, the profile of the stationary electric field takes three types of roots. At first, all stationary electric fields in the radial points takes the electron root ($E_r > 0$). Secondly, when the density increases, the stationary electric field in the core plasma takes the electron root and the electric field in the outer plasma takes the ion root ($E_r < 0$). Furthermore, in this case, the type of the transition is classified to the soft or hard one. When the value of the density becomes much larger ($\bar{n} \approx 10^{20}\mathrm{m}^{-3}$), all radial stationary electric fields take the ion root. The parameter region of the three root patterns of the stationary electric field is shown in the $\bar{n} - \bar{T}_e/\bar{T}_i$ plane. The multiple solutions are obtained in the region: $\bar{T}_e/\bar{T}_i \approx 2$ and $\bar{n} = (2-7) \times 10^{18}\mathrm{m}^{-3}$. In this region, the hard transition occurs between the multiple solutions and the reduction of the anomalous conductivity is found due to the strong gradient of the radial electric field. In the region where the electron root and the ion root co-exist outside this region, the spatial soft transition occurs without the multiple solutions.

4.3. Solutions by use of the machine parameters of LHD

We next study the case by use of the machine parameters of LHD. We choose the case that the absolute power is 500W. We set the electron heating is 1MW and the particle source term $S_0 = 2 \times 10^{24}\mathrm{m}^{-3}\mathrm{s}^{-1}$. The stationary solutions of the radial electric field are obtained for $\bar{n} = 4 \times 10^{18}\mathrm{m}^{-3}$, $\bar{T}_e = 1600\mathrm{eV}$ (T_e at the center: $T_e(0) = 4200\mathrm{eV}$) and $\bar{T}_i = 800\mathrm{eV}$ (T_i at the center: $T_i(0) = 2200\mathrm{eV}$). The other parameters are same as those in Sec 4.1. The ratio of the electron temperature of the ion temperature takes the value $\bar{T}_e/\bar{T}_i \approx 2$. The profile of the stationary radial electric field is shown in figure 2(a). The multiple solutions (open marks in figure 2(a)) exist and the gradient of the electric field is strong enough to suppress the turbulence: $|E_r'| = 8.5 \times 10^5 V/m^2$. Therefore, the reduction of the anomalous heat conductivity is found in the parameter region examined here in figure 2(b). The reduction of χ_a is smaller than that in the case by use of CHS device parameters. The value of the reduction depends on the choice of the model of the anomalous heat conductivity. The test of the anomalous heat conductivity will be done by the experiment in LHD. In the other parameter regimes, *e.g.*, $\bar{T}_e/\bar{T}_i \approx 9$, the multiple solutions do not exist and the transition is found to occur smoothly from electron root to the ion root. Detailed study in the wide parameter is needed by use of the LHD typical device parameters.

5. Summary and Discussions

In this paper, the structure of the radial electric field in helical plasmas is theoretically studied. Theoretical model of the ballooning mode or the interchange mode is adopted for the anomalous heat conductivity and the anomalous diffusion coefficient of the electric field. At first, the typical machine parameters of CHS are adapted. The hard transition of the E_r structure between the multiple ambipolar E_r is obtained in this study of $T_e/T_i \approx 2$. When $T_e/T_i \approx 3$ and the value of the density takes about $1 \times 10^{19}\mathrm{m}^{-3}$, the transition type is found to become soft (without multiple ambipolar E_r). The condition for the suppression of the anomalous diffusivities is suggested to be rather high T_i in addition to the low density and high T_e. Next, the typical machine parameters of LHD are used. The hard transition (with the multiple solutions of E_r) is shown in the E_r structure in the parameter region examined here.

In CHS device, the spatial transition from the larger positive E_r to the smaller positive E_r is observed [1]. Such a spatial transition dose not induce a local peak of χ_j^{NEO}, and should be searched for in simulations. The study by use of the LHD typical machine parameters is necessary to show the region in which the multiple solutions of ambipolar E_r exist in the phase diagram of the $\bar{n} - \bar{T}_e/\bar{T}_i$ plane. These are left for future studies.

Acknowledgments

The authors would like to acknowledge Prof. S. -I. Itoh, Prof. A. Fukuyama and Dr. M. Yagi for illuminating discussions. In particular, one of the authors (ST) thanks Prof. A. Fukuyama for helpful suggestions relating to the numerical methods. Discussions with Dr. A. Fujisawa, Dr. K. Ida, Dr. H. Sanuki and Dr. H. Sugama are also appreciated.

This work is partly supported by a Grant-in-Aid for Scientific Research from the Ministry of Education, Culture, Sports, Science and Technology of Japan.

[1] Fujisawa A *et al* 2000 Phys. Plasmas **7** 4152
[2] Kovriznykh L M 1984 Nucl. Fusion **24** 851
[3] Ida K 1998 Plasma Phys. Control. Fusion **40** 1429
[4] Toda S and Itoh K 2001 Plasma Phys Control. Fusion **43** 629
[5] Toda S and Itoh K 2001 *28th EPS Conf on Control. Fusion and Plasma Phys. (18-22 June 2001, Funchal, Portugal)* P4.055
[6] Itoh K, Itoh S -I, Fukuyama A, Sanuki H and Yagi M 1994 Plasma Phys. Control. Fusion **34** 123
[7] Shaing K C 1984 Phys. Fluids **27** 1567
[8] Hastings D E 1985 Phys. Fluids **28** 334
[9] Itoh K, Itoh S -I, Fukuyama A, Yagi M and Azumi M 1994 Plasma Phys. Control. Fusion **36** (1994) 279
[10] Yamada H *et al* 2001 *28th EPS Conf. on Control. Fusion and Plasma Phys. (18-22 June 2001, Funchal, Portugal)* IT.05, to be published in Plasma Phys. Control. Fusion
[11] Itoh K, Itoh S -I, Fukuyama A, Yagi M and Azumi M 1993 J. Phys. Soc. Jpn. **62** 4269

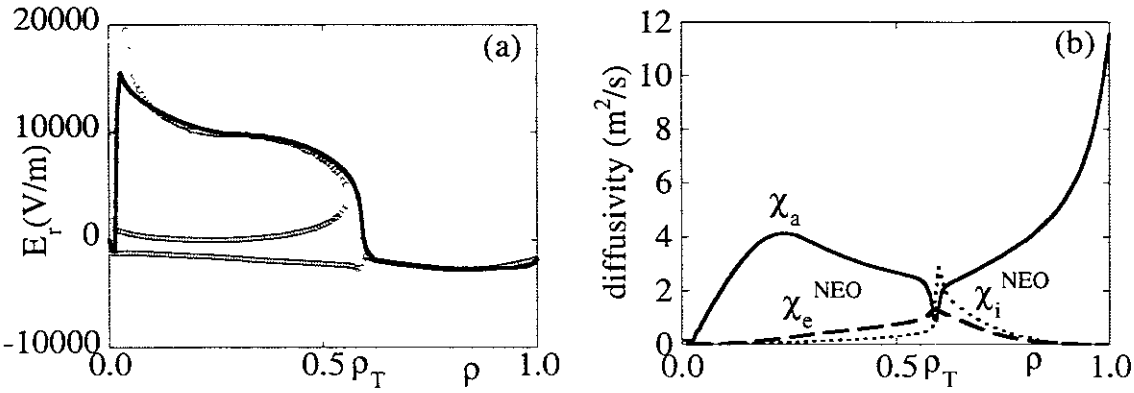

Figure 1. (a) Radial dependence of the electric field (full curve). Open circles show the values of the ambipolar electric field. (b) Radial dependence of the diffusivities. The suppression of the anomalous diffusivity is obtained due to the strong gradient of the electric field. The absorbed power of electrons is 100kW and that of ions is 50kW, respectively. The coefficient S_0 of the particle source is $7 \times 10^{24}\mathrm{m}^{-3}\mathrm{s}^{-1}$. The result in figure 1 is derived by use of the CHS typical parameters.

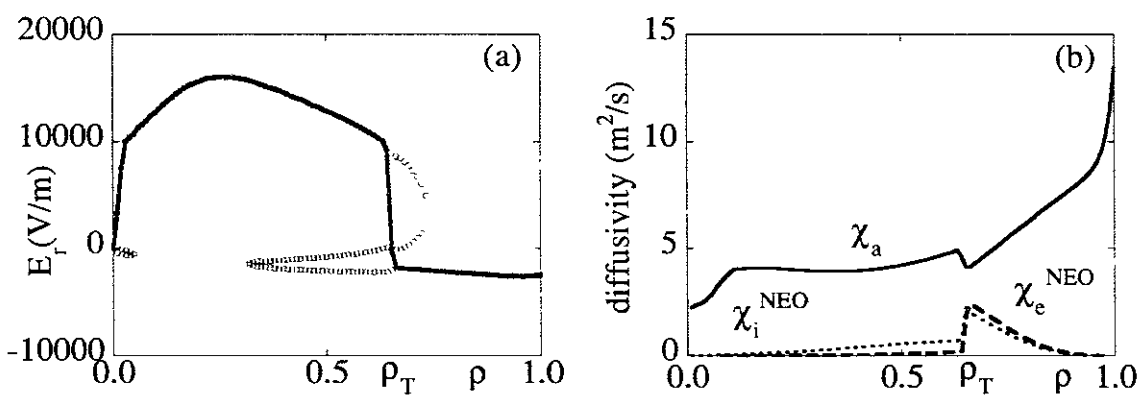

Figure 2. (a) Radial dependence of the electric field (full curve). Open circles show the values of the ambipolar electric field. The multiple solutions are obtained in the parameter regime examined here. (b) Radial dependence of the diffusivities. The absorbed power of electrons is 1MW and that of ions is 500kW, respectively. The coefficient S_0 of the particle source is $2 \times 10^{24}\mathrm{m}^{-3}\mathrm{s}^{-1}$. The result in figure 2 is derived by use of the LHD typical parameters.

Transition Probability to Turbulent Transport Regime

Mitsuhiro Kawasaki, Atsushi Furuya**, Masatoshi Yagi,
Kimitaka Itoh** and Sanae-I. Itoh

Research Institute for Applied Mechanics, Kyushu University,
Kasuga 816-8580, Japan
*Interdisciplinary Graduate School of Engineering Sciences,
Kyushu University, Kasuga 816-8580, Japan
**National Institute for Fusion Science, Toki 509-5292, Japan

Abstract

Transition phenomena between thermal noise state and turbulent state observed in a submarginal turbulent plasma are analyzed with statistical theory. Time-development of turbulent fluctuation is obtained by numerical simulations of Langevin equation which contains hysteresis characteristics. Transition rates between two states are analyzed. Transition from turbulent state to thermal noise state occurs in entire region between subcritical bifurcation point and linear stability boundary.

1 Introduction

There have been observed various kinds of formations and destructions of transport barriers. Both in edge and internal regions of high temperature plasmas, the dynamical change often occurs on the short time scale, sometimes triggered by subcritical bifurcation. These features naturally lead to the concept of transition.

The transition takes place as a statistical process in the presence of statistical noise source induced by strong turbulence fluctuation. As the generic feature the transition occurs with a finite probability when a parameter approaches the critical value.

The nonequilibrium statistical mechanics, which deals with dynamical phase transitions and critical phenomena, should be extended for inhomogeneous plasma turbulence [1]. To this end, statistical theory for plasma turbulence has been developed and stochastic equations of motion (the Langevin equations) of turbulent plasma were derived [2]. The framework to calculate the probability density function (PDF), the transition rates etc. have also been made.

In this paper, we apply the theoretical algorithm to an inhomogeneous plasma with the pressure gradient and the shear of the magnetic field. Micro turbulence is known to be subcritically excited from the thermal noise state [3]. The transition between thermal noise state and turbulent state is studied. We show that the transition occurs stochastically by numerically solving the Langevin equation of the turbulent plasmas. In order to characterize the stochastic nature of the transition, the frequency of occurence of a transition per unit time (the transition rates) are calculated as a function of the pressure-gradient and the plasma temperature. The results show that the transition from the turbulent state to the thermal noise state occurs in a wide region instead of at a transition point.

2 Theoretical Framework

In this section, we briefly review the theoretical framework [2] used in our analysis of turbulent plasmas.

The theory is based on the Langevin equation Eq. (1) derived by renormalizing with the direct-interaction approximation the reduced MHD for the three fields: the electro-static potential, the current and the pressure.

$$\frac{\partial \mathbf{f}}{\partial t} + \hat{\mathcal{L}}\mathbf{f} = \mathcal{N}(t), \text{ where } \mathbf{f}(t) \equiv \begin{pmatrix} \phi(t) \\ J(t) \\ p(t) \end{pmatrix}. \tag{1}$$

Since $\mathcal{N}(t)$ is a force which fluctuates randomly in time, the Langevin equation describes the stochastic time-development of the fluctuation of the three fields.

By analyzing the Langevin equation Eq. (1), a number of statistical properties of turbulent plasmas can be derived. For example, it was shown that asymptotic forms of the probability distribution functions for the energy of the fluctuation of the electric field obeys a power-law. The analytical formulae of the rate of change of states of plasmas, the transition rates, were also derived. Furthermore, since the renormalized transport coefficients come from the term of the random force $\mathcal{N}(t)$, relations between the fluctuation

levels of turbulence and the transport coefficients like the viscosity and the thermal diffusivity were derived.

3 A Model

With the theoretical framework briefly described in the previous section, we analyze a model of inhomogeneous plasmas with the pressure-gradient and the shear of magnetic field [2]. The model is formulated with the reduced MHD of the three fields of the electro-static potential, the current and the pressure. The shear of magnetic field is given as $\mathbf{B} = (0, B_0 sx, B_0)$ where $B_0(x) = \text{const} \times (1 + \Omega' x + \cdots)$. The pressure is assumed to change in $x-$direction.

It has been known that in this system bifurcation due to the subcritical excitation of the current diffusive interchange mode (CDIM) occurs [3] as shown in Fig. (1). Figure (1) shows the pressure-gradient dependence of

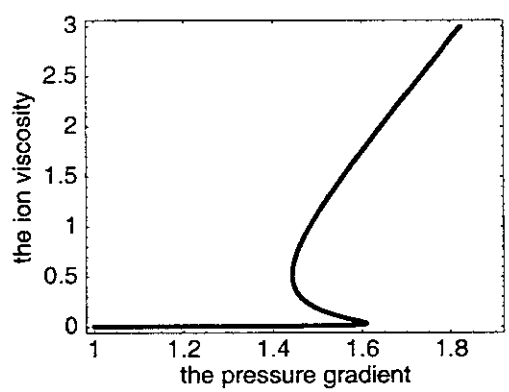

Figure 1: The pressure-gradient dependence of the renormalized ion-viscosity. It is clearly seen that the bifurcation between a low viscosity state (the thermal noise state) and a high viscosity state (the turbulent state) occurs.

the turbulent ion-viscosity which is proportional to the fluctuation level. It is clearly seen that the bifurcation between a low viscosity state and a high viscosity state occurs. Due to the bifurcation, transition between the two states and hysteresis are expected to be observed. We call the low viscosity state "the thermal noise state", since in this state the system fluctuates with thermal noise considered in the model [4]. We call the high viscosity state "the turbulent state", since the fluctuation level is also large in a strong turbulent limit [2]. The ridge point where the turbulent branch ends is denoted

"the subcritical bifurcation point". The region between the subcritical bifurcation point and the ridge near the linear stability boundary is called "the bi-stable regime".

From the deterministic point of view, the transition from the thermal noise state to the turbulent state is expected to occur at the ridge point near the linear stability boundary and the transition in the opposite direction is expected to occur at the subcritical bifurcation point.

4 Stochastic Occurence of the Transition

In order to capture the characteristics of the two states, we concentrate on the time-development of the energy of fluctuation of the electric field, $\varepsilon(t)$. The quantity $\varepsilon(t)$ obeys the coarse-grained Langevin equation Eq. (2) which has been derived in [2].

$$\frac{d}{dt}\varepsilon(t) = -2\Lambda(\varepsilon)\varepsilon(t) + \eta(\varepsilon)R(t). \tag{2}$$

Here, $R(t)$ is the Gaussian white noise. For the detailed formulae of $\Lambda(\varepsilon)$ and $\eta(\varepsilon)$, see [4]. The essential point is that the function $\Lambda(\varepsilon)$ takes both a positive and a negative value in the bi-stable regime. So, the fluctuation of the electric field is suppresed when Λ is positive and it is excited when Λ is negative. Consequently, there are two metastable states in the bi-stable regime. In addition, $\eta(\varepsilon)$ is a positive function.

By solving numerically Eq. (2), we obtain the following samples of a time serieses. When the pressure-gradient is fixed at the value smaller than the subcritical bifurcation value, as shown in Fig. (2), there is only smal fluctuation since the system is always in the thermal noise state.

On the other hand, when the pressure-gradient takes a value in the bi-stable regime, bursts are observed intermittently as shown in Fig. (3). That is, transition between the thermal noise state and the turbulent state occurs *stochastically*. The bursts corresponds to the turbulent state and the laminar corresponds to the thermal noise state. The fact that the residence times at the each states are random leads to the statistical description of the transition with the transition rates described in the next section.

When the value of the pressure-gradient is larger than that of the linear stability boundary (see Fig. (4)), bursts are always observed. It means that the system is always in the turbulent state.

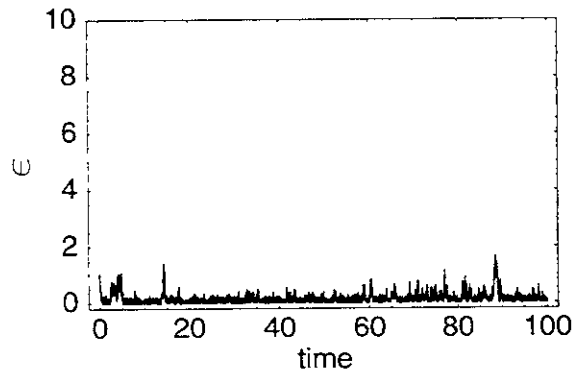

Figure 2: A sample of a time-series of the energy of fluctuation of the electric field $\varepsilon(t)$ when the pressure-gradient is fixed at the value smaller than that of the subcritical bifurcation point. There is only small fluctuation since the system is always in the thermal noise state.

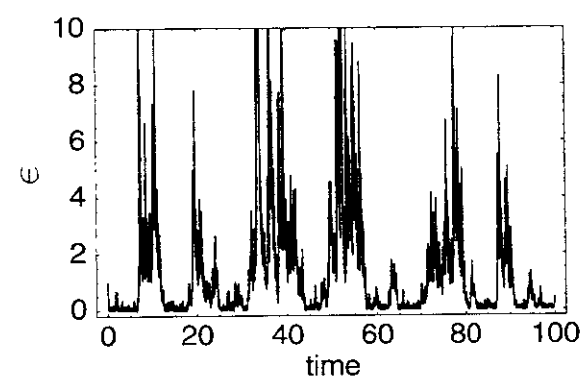

Figure 3: A sample of a time-series of $\varepsilon(t)$ when the pressure-gradient takes a value in the bi-stable regime. Bursts are observed intermittently. It means the transition between the thermal noise state and the turbulent state occurs stochastically.

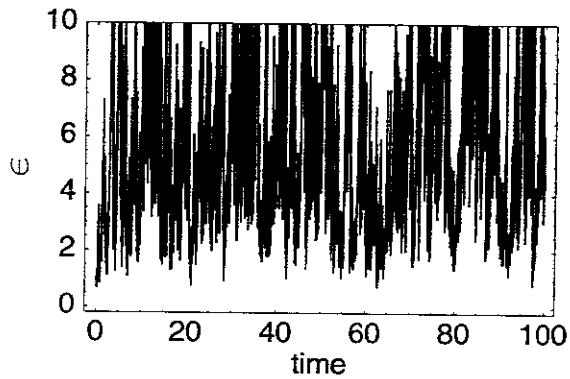

Figure 4: A sample of a time-series of $varepsilon(t)$ when the value of the pressure-gradient is larger than that of the linear stability boundary. Bursts occurs simultaneously since the system in the turbulent state.

5 The Transition Rates

In order to formulate the above stochastic transition phenomena in the bi-stable regime, we introduce the transition rates. There are transtions in two opposite direction: the transition from the thermal noise state to the turbulent noise state, which we call "the forward transition, and the transition in the opposite direction is called "the backward transition". There are two transition rates. One is the forward transition rates r_f which is the frequency of occurence of the forward transition per unit time and the other is the backward transition rate r_b defined similarly as the frequency of occurence of the backward transition per unit time.

It is important to note that these quantities are observable quantities. It is easily shown that the forward transition rate is equal to the average of inverse of the residence time at the thermal noise state and the backward transition rate is equal to the average of inverse of the residence time at the turbulent state. Therefore, these transition rates can be measured from the time serieses of fluctuation.

We analyze in which region of the value of the pressure-gradient the transtion occurs frequently. The transition rates are calculated with the formulae derived in [5]. The two figures, Fig. (5) and Fig. (6), show pressure-gradient dependence of the forward transition rate and the backward transition rates in the bi-stable regime. The forward transition triggered by the thermal noise occurs mainly in the vicinity of the linear stability boundary. In contrast to that, it is clearly seen that the backward transition occurs in the almost entire bi-stable regime. This behavior is due to strong turbulent

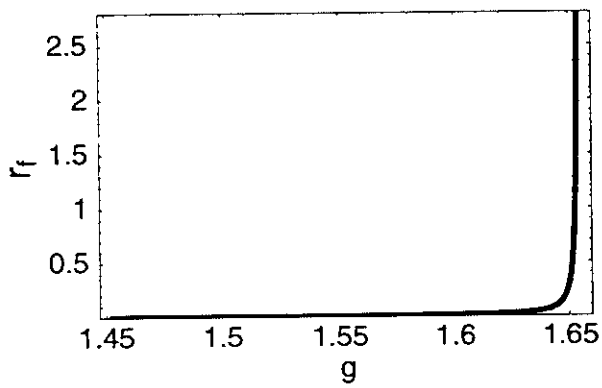

Figure 5: The pressure-gradient (g) dependence of the forward transition rate in the bi-stable regime. The left edge and the right edge of the horizontal axis corresponds to the subcritical bifurcation point and the linear stability boundary. It is seen that the forward transition occurs mainly in the vicinity of the linear stability boundary.

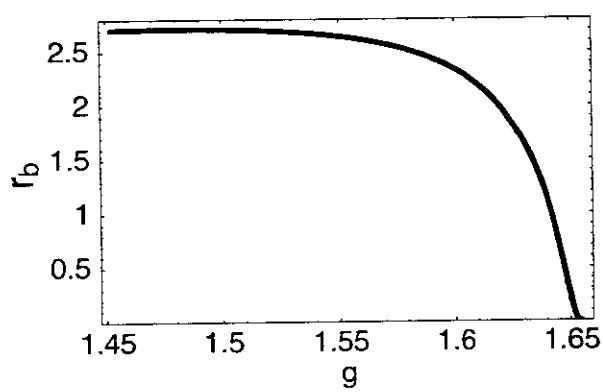

Figure 6: The pressure-gradient dependence of the backward transition rate in the bi-stable regime. It is seen that the backward transition occurs in the almost entire bi-stable regime.

fluctuation. It is noted that the backward transition, i.e. the transition in a turbulence, occurs in a "region" instead of a "point".

6 Summary

Summarizing our work, we applied the statistical theory of plasma turbulence to problems of the transition phenomena of submarginal turbulence. By numerically solving the Langevin equation, typical time-development of fluctuation is obtained. It tells that the transition for the model of inhomogeneous plasma occurs stochastically and suggests how the transition phenomena due to subcritical bifurcation may look in time-serieses obtained in real experiments. Furthermore, we obtained pressure-gradient dependence of the transition rates. It is shown that the backward transition occur with almost equal frequency in the entire bi-stable regime, so the transition occurs in a "region". The concept "transition region" is necessary in the analysis of data obtained by real experiments.

References

[1] See, e.g., Kubo R, Toda M and Hashitsume N 1985 *Statistical Physics II* (Springer, Berlin); Balescu R 1975 *Equilibrium and Nonequilibrium Statistical MEchanics* (Wiley).

[2] Itoh S-I and Itoh K 1999 J. Phys. Soc. Jpn. **68** 1891; **68** 2611; **69** 408; **69** 427; **69** 3253.

[3] Itoh K, Itoh S-I, Yagi M and Fukuyama A 1996 Plasma Phys. Control. Fusion **38** 2079.

[4] Itoh S-I and Itoh K 1999 J. Phys. Soc. Jpn. **68** 2611.

[5] Itoh S-I and Itoh K 2000 J. Phys. Soc. Jpn. **69** 427.

Multiple bifurcation of the radial electric field structure induced by electrodes in tokamaks

N. Kasuya, K. Itoh[1], Y. Takase[2]

Graduate School of Science, University of Tokyo, Tokyo, Japan
1 National Institute for Fusion Science, Toki, Japan
2 Graduate School of Frontier Sciences, University of Tokyo, Tokyo, Japan

Abstract.

An improved confinement state can be attained by imposing a radial electric field at the plasma edge. This is characterized by a change of the radial electric field structure. A charge conservation equation with a diffusion term has been solved to explain this mechanism. When the distance between electrodes is finite, various types of radial electric field structures with multiple peaks are allowed for the same boundary condition. The distance between electrodes determines the number of possible solutions. The relationship between the voltage and the current is obtained by numerical calculation. Both stable and unstable regions exist in the stationary solutions and their boundary points are critical points for transition from one state to another. Multiple transitions and hysteresis are predicted. The magnitude of the collision frequency affects the existence of multiple solitary solutions.

1.Introduction

The steep gradient of the electric field and the self-sustaining mechanism of its structure are key issues in physics of H-mode and improved confinement states. Radial electric field structure bifurcation,[1] which has a variation of the radial direction, and poloidal shock,[2] which has a variation of the poloidal direction are both studied theoretically. Various measurements have been carried out to understand the radial electric field structure bifurcation.[3,4,5]

The transition from L-mode to H-mode is characterized by a sudden change of the radial electric field structure. An improved confinement state can also be attained by imposing a radial electric field at the plasma edge.[3,4,6,7] The H-mode has been attained by inserting an electrode into the plasma and applying a voltage. This method provides a controllable way of attaining an improved confinement state. In TEXTOR biasing experiments the spatial profile of the radial electric field at the plasma edge changed from a flat one before the transition to a peaked one after the transition.[4]

There are several theories that can explain the characteristic structure of the radial electric field[8-15] (see Ref.15 for a review). The case of infinite distance between

electrodes and of finite distance with a simplified conductivity model were described in Ref.13 and Ref.14, respectively. Solitary radial electric field structures were derived in these references. An extension of the work of Ref.14 with the conductivity that has the form of the imaginary part of the plasma dispersion function is described in this paper.

2.Model equation

The essence of the method for obtaining the radial electric field structure was described in Ref.13. The first step combines the Poisson's equation and the charge conservation law to obtain

$$\frac{\partial}{\partial t}E_r = -\frac{1}{\varepsilon_0\varepsilon_\perp}(J_r - \varepsilon_0\varepsilon_\perp \nabla\cdot\mu_i\nabla E_r - J_{ext}), \tag{2.1}$$

where J_r is the local current, μ_i is the shear viscosity of ions, J_{ext} is the current driven into the electrode by the external circuit, ε_0 is the vacuum susceptibility, and $\varepsilon_\perp$ is the dielectric constant of a magnetized plasma. The local current is determined by the radial electric field at the same radial location. The second term of the right hand side of eq.(2.1) acts as a diffusion term due to anomalous shear viscosity. Anomalous transport is ambipolar in the lowest order, and it influences the radial electric field through ion viscosity.

In stationary state a normalized form of the equation can be written as,

$$\frac{\partial^2}{\partial x^2}X - f(X,y)X + I = 0, \tag{2.2}$$

where $X=e\rho_p E_r/2T_i=E_r/(v_{ti}B_\theta)$, $I=(e\rho_p/T_i\sigma(0))J_{ext}$, $x=(r-r_0)/l$, $l=\sqrt{\mu_i\varepsilon_0\varepsilon_\perp/\sigma(0)}$ and $y=rv_{ii}B/v_{ti}B_\theta$. In the definition above, X is the normalized radial electric field, I is the normalized external current, x is the radius normalized by l, y is the normalized collision frequency, $\sigma(0)$ is the conductivity when the radial electric field is zero, ρ_p is the ion poloidal gyroradius, T_i is the ion temperature, v_{ti} is the ion thermal velocity and v_{ii} is the ion collision frequency. The radius r_0 is chosen to be the mid-point between the two electrodes. This radial electric field equation is a nonlinear differential equation. Here all parameters that do not involve the radial electric field are treated as constants in space for simplicity. We are interested in the steep gradient of the radial electric field, and therefore neglect the spatial variation of other slowly varying parameters. In eq.(2.2) $f(X,y)$ is a function that relates the conductivity and the radial electric field,

$$J_r = \sigma(E_r)E_r = \sigma(0)f(X,y)E_r, \tag{2.3}$$

where $\sigma(E_r)$ is the conductivity when the radial electric field is E_r.

If anomalous transport is ambipolar in the lowest order, the radial current is determined by neoclassical transport, mostly of ions. The radial current, which is induced by the neoclassical transport process, has a dependency on the imaginary part of $Z(X,y)$ [$=ImZ(X,y)$], where $Z(X,y)$ is the plasma dispersion function. Here we take

$$f(X,y) = Im\,Z(X,y), \tag{2.4}$$

$$Z(X,y) = \frac{1}{\pi^{1/2}}\int_{-\infty}^{\infty}\frac{\exp(-t^2)}{t-z}dt, \quad (z \equiv X + iy), \tag{2.5}$$

for simplicity, though the ambipolar electric field and other components affect the radial current. That is because we are interested in capturing the physical basis, not in explaining the details of experiments.

3.Solitary solutions

To solve eq.(2.2), the boundary condition at the position of electrodes is chosen to be $\partial X/\partial x = 0$. One half of the distance between electrodes is denoted d.

Equation (2.2) has spatially constant solutions X1 and X2, which satisfy $X\,f(X,y) - I = 0$. Other than these trivial solutions, solitary solutions are obtained by solving eq.(2.2) numerically. Figure 1 shows an example of the spatial profile of the radial electric field structure. Since eq.(2.2) has transition invariance in space, two solutions for half the distance between electrodes joined in series, is also a solution with the boundary condition $\partial X/\partial x = 0$. In this way solutions with many peaks can exist when the distance d is finite.

There exists the minimum distance between electrodes for a solitary solution of eq.(2.2) to exist. This distance was calculated in Ref.14 for the case when a simplified form of function f(X,y) was adopted. In the same way, the minimum distance is given by

$$d_{min} = \pi/\sqrt{|g|}, \tag{3.1}$$

where we take $g \equiv \{\partial[Xf(X,y)]/\partial X\}_{X=X2}$. This quantity determines the maximum number of peaks that a solitary solution can have. In the case of Fig.1 the maximum number of the peaks is three.

The shape of the solitary solution is affected by physical parameters, such as the viscosity and the conductivity. Measurement of this structure gives information on those parameters.

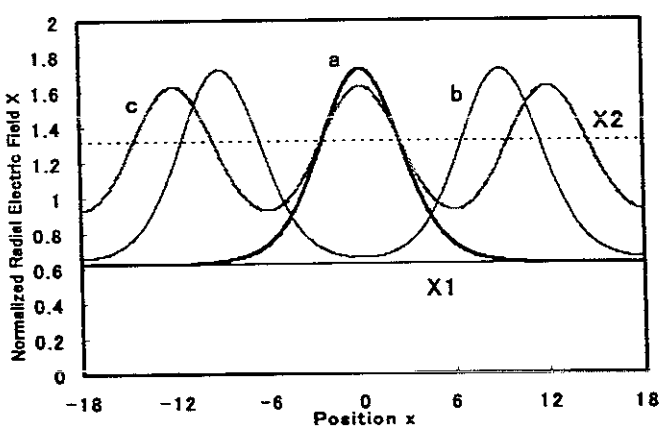

Fig.1 Solitary structures of the radial electric field when $d=18$, $y=0.1$ and $I=0.5$. a, b

and c are solutions that have one, two and three peaks, respectively.

4.Multiple transitions

Integrating $X(x)$ obtained in the previous section gives the voltage between electrodes,

$$V = \int_{-d}^{d} X(x)dx . \tag{4.1}$$

The voltage V can be calculated for a given current I numerically.

Figure 2 shows $V - I$ curves for the case of $d=18$ and $y=0.1$. The spatially constant solutions X1 and X2 exist on the branches T1 and T2, respectively. S1~S3 are solutions having solitary structures. S1 has one peak, S2 has two peaks, and so on. Solutions that have more than three peaks are not allowed for this choice of d because the minimum peak width is given by eq.(3.1).

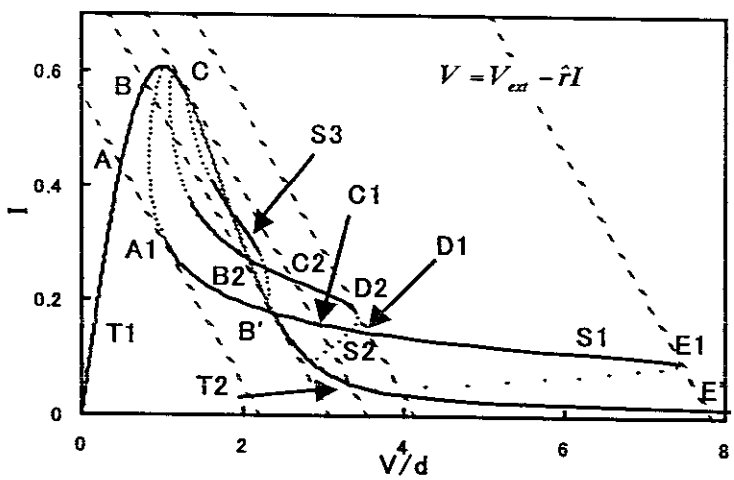

Fig.2 The relationship between voltage and current. A~E, A1, B', etc. denote intersections with or points of tangency to the line $V = V_{ext} - \hat{r}I$ plotted as dashed lines. Solid lines are stable and dotted lines are unstable in each branch. This is the case when $d=18$, $y=0.1$ and $\hat{r}=4.0$.

The parameters V and I are determined by the intersection of the solutions T1, T2, S1~S3 and the circuit equation

$$V = V_{ext} - \hat{r}I , \tag{4.2}$$

where $\hat{r}$ is the internal resistance of the external circuit. The voltage V is that across the plasma, and V_{ext} is the applied voltage between electrodes. If the externally supplied voltage V_{ext} is varied, the values of V and I change accordingly.

Among the obtained solutions, both stable and unstable solutions exist. Stability of the solutions is evaluated by eq.(2.2) with an additional time derivative

term. When a perturbation is given to the radial electric field, that is $X(x) \to X(x) + \tilde{X}$, the linearized equation for the perturbation is given as

$$\frac{\partial}{\partial \tau}\tilde{X} = \frac{\partial^2}{\partial x^2}\tilde{X} - \frac{\partial}{\partial X}[X f(X,y)]\tilde{X} - \frac{1}{\hat{r}d}\int_0^d \tilde{X}dx = \lambda \tilde{X}, \tag{4.3}$$

where τ is the time normalized by $t_N = \varepsilon_0 \varepsilon_\perp / \sigma(0)$ and λ corresponds to the growth rate of perturbation. The electrode current I depends on the electric field in the entire range between electrodes, so that its perturbation becomes the integral of $\tilde{X}$, as denoted in eq.(4.3). Noted that perturbed quantities must be held under the constraint of the circuit equation eq.(4.2). Equation (4.3) is solved as an eigenvalue problem. The integral of $\tilde{X}$ in eq.(4.3) acts as a stabilizing term. Figure 3 shows the dependence of the maximum growth rate on the current I for the same case as Fig.2. It shows that it becomes unstable at larger and smaller current. The points where the maximum growth rate is zero give the boundaries between stable and unstable regions, and they correspond to the points of tangency to the circuit relation on the solitary solution branch S1~S3.

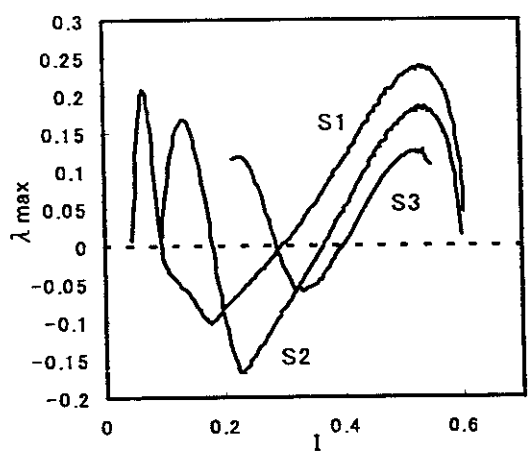

Fig.3 The maximum growth rate plotted as a function of the current I for the case of $d=18, y=0.1$ and $\hat{r}=4.0$. S1~S3 denote the solutions that have 1~3 peaks, respectively.

Solid lines are stable and dotted lines are unstable in Fig.2. The entire region of T1 is stable but some region of T2 is unstable given the constraint of $V = V_{ext} - \hat{r}I$. The boundary point is the point of tangency to the line $V = V_{ext} - \hat{r}I$ with appropriate V_{ext}. When V_{ext} is small, only one intersection exists on T1. For larger V_{ext}, an intersection can exist on S1 (one peak solution). The transition from a constant solution to a solitary one occurs at the critical point C. In the case shown in Fig.2 the tangential line at C intersects with S1, S2 and T2. Which solution is taken after the transition depends on the stability of the solution. If solution S2 is taken, the next transition to S1

will occur at D2, and the next at E1 to the constant solution T2 takes place. In this way multiple transitions are possible for a range of resistance $\hat{r}$. For different $\hat{r}$, the number of intersections that the tangential line at C has with solitary solutions is different. When the resistance is much larger, transitions to solitary solutions cannot take place and only transition from a constant solution to another constant solution takes place. In contrast, when the resistance is much smaller, the entire range of T2 becomes stable and transitions are not possible. The number of transition steps depends on the value of the resistance $\hat{r}$. In case of Fig.2 ($d=18$) transitions can take place four times at most.

When V_{ext} decreases from point E' on T2, a back transition can take place at B', and multiple back transitions can occur. These back transition points are not the same as the forward transition points, so that there is a hysteresis in the electric field structure as a function of the applied voltage.

5.Effects of collision

The transitions shown in the previous section are for the case of $y=0.1$ when ion-ion collision is not effective. The collision frequency affects the solitary structure through the function $f(X,y)=ImZ(X,y)$. Figure 4(a) shows the $V-I$ curve for the collisional case ($y=5.0$). The existence range of solitary solutions becomes smaller than in the collisionless case. In the collisionless limit, neoclassical transport is dominated by the resonant particles which satisfy $v_{\parallel}B_{\theta} \sim E_r$, so that neoclassical radial current $Xf(X,y)$ has a large maximum at $X=1$. For the collisional case the collisional effect on neoclassical transport is dominant for radial electric field X larger than one, so that the neoclassical radial current $X\,f(X,y)$ has a broader profile.[8,16] Figure 4(b) is a plot of d_{min}, which is the minimum distance between electrodes for a solitary solution to exist, deduced from eq.(3.1). Increasing the viscosity y leads to larger d_{min} at the same current I. Solitary solutions have a finite curvature $\partial^2 X/\partial x^2$, which is sustained by the neoclassical radial current from eq.(2.2). When the collision frequency y is large, the gradient of $Xf(X,y)$ becomes close to zero, so that the variation of the radial electric field makes little change in the neoclassical radial current. Therefore, the curvature of the solitary solution cannot be sustained when y is large. This is why solitary solutions are hard to exist in the collisional case.

(a) (b)

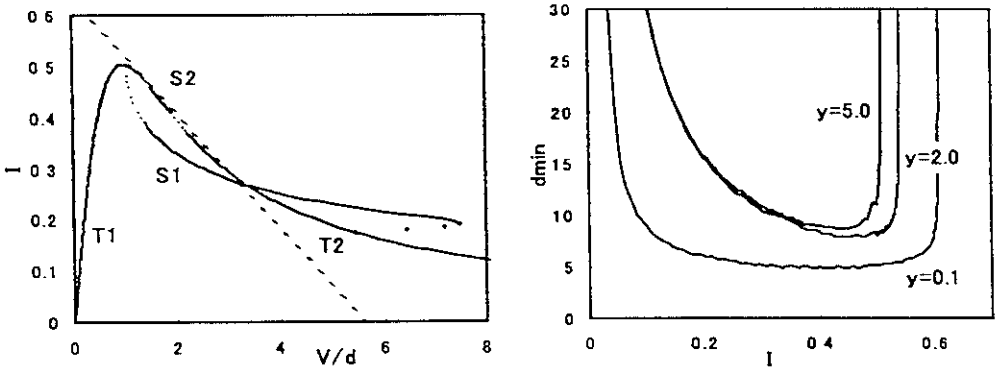

Fig4. (a) is the relationship between the voltage and the current when $d=18$ and $y=5.0$, which is the collisional case. (b) is the minimum distance between electrodes for a solitary solution to exist when $y=0.1$, 2.0 and 5.0.

6.Summary

The radial electric field structure is derived from a charge conservation equation with a diffusion term. An extension to the case of finite distance between electrodes and using $f(X,y)$ with the form of $ImZ(X,y)$ is carried out. In this case various types of radial electric field structures with multiple peaks are allowed for the same boundary condition. The distance between electrodes determines the number of solutions for a given applied voltage. There is a minimum distance for solitary solutions to exist. Both stable and unstable regions exist in the stationary solutions, and their boundary points give critical points for transition from one state to another. The existence of many solutions predicts the possibility of multiple transitions and hysteresis. The magnitude of the collision frequency affects the existence of multiple solitary solutions. In the collisional case the range where solitary solutions exist is narrow, so that transitions to solitary structures are less likely to take place. Nonlinear response functions could be interpreted from the radial electric field structure and its bifurcation.

Basic properties such as peaked structures of the radial electric field and transitions in the V-I relationship can be explained. However, some features of experimental results[3], such as the asymmetry between positive and negative biasing, are not reproduced. Components neglected in this work, such as the neoclassical ambipolar electric field, must be included for a more quantitative comparison.

List of captions for figures

Fig.1 Solitary structures of the radial electric field when $d=18$, $y=0.1$ and $I=0.5$. a, b and c are solutions that have one, two and three peaks, respectively.

Fig.2 The relationship between voltage and current. A~E, A1, B', etc. denote intersections with or points of tangency to the line $V = V_{ext} - \hat{r}I$ plotted as dashed lines. Solid lines are stable and dotted lines are unstable in each branch. This is the case when $d=18$, $y=0.1$ and $\hat{r}=4.0$.

Fig.3 The maximum growth rate plotted as a function of the current I for the case of $d=18$, $y=0.1$ and $\hat{r}=4.0$. S1~S3 denote the solutions that have 1~3 peaks, respectively.

Fig4. (a) is the relationship between the voltage and the current when $d=18$ and $y=5.0$, which is the collisional case. (b) is the minimum distance between electrodes for a solitary solution to exist when $y=0.1$, 2.0 and 5.0.

List of References

[1] S. –I. Itoh, K. Itoh, A. Fukuyama et al.: Phys. Rev. Lett. 67 (1991) 2485.
[2] K. C. Shaing, R. D. Hazeltine and H. Sanuki: Phys. Fluids B4 (1992) 404.
[3] R. R. Weynants, G. Van Oost, G. Bertschinger et al.: Nucl. Fusion 32 (1992) 837.
[4] J. Boede, D. Gray, S. Jachmich et al.: Nucl. Fusion 40 (2000) 1397.
[5] K. Ida and N. Nakajima: Phys. Plasmas 4 (1997) 310.
[6] R. J. Taylor, M. L. Brown, B. D. Fried et al.: Phys. Rev. Lett. 63 (1989) 2365.
[7] L. G. Askinazi, V. E. Golant, S. V. Lebedev et al.: Nucl. Fusion 32 (1992) 271.
[8] T. E. Stringer: Nucl. Fusion 33 (1993) 1249.
[9] J. Cornelis, R. Sporken, G. Van Oost and R. R. Weynants: Nucl. Fusion 34 (1994) 171.
[10] D. E. Hastings, R. D. Hazeltine and P. J. Morrison: Phys. Fluids 29 (1986) 69.
[11] P. H. Diamond, V. B. Lebedev, D. E. Newman et al.: Phys. Plasmas 2 (1995) 3685.
[12] J. A. Heikkinen, S. Jachmich, T. P. Kiviniemi et al.: Phys. Plasmas 8 (2001) 2824.
[13] K. Itoh, S. –I. Itoh, M. Yagi, and A. Fukuyama, Phys. Plasmas 5 (1998) 4121.
[14] N. Kasuya, K. Itoh and Y. Takase; to be published in J. Phys. Soc. Japan.
[15] K. Itoh, S.-I. Itoh and A. Fukuyama: Transport and Structural Formation in Plasmas (IOP, England, 1999).
[16] J. W. Connor and T. E. Stringer: Phys. Fluids 14 (1971) 2184.

Recent Issues of NIFS Series

NIFS-689 A Maluckov, N Nakajima, M Okamoto, S Murakami and R Kanno,
Statistical Properties of the Neoclassical Radial Diffusion in a Tokamak Equilibrium Apr 2001

NIFS-690 Y Matsumoto, T Nagaura, Y Itoh, S-I Ohkawa and T Watanabe,
LHD Type Proton-Boron Reactor and the Control of its Peripheral Potential Structure Apr 2001

NIFS-691 A Yoshizawa, S -I Itoh, K Itoh and N Yokoi,
Turbulence Theories and Modelling of Fluids and Plasmas Apr 2001

NIFS-692 K Ichiguchi, T Nishimura, N Nakajima, M Okamoto, S -i Ohkawa, M Itagaki,
Effects of Net Toroidal Current Profile on Mercier Criterion in Heliotron Plasma. Apr 2001

NIFS-693 W Pei, R Horiuchi and T Sato,
Long Time Scale Evolution of Collisionless Driven Reconnection in a Two-Dimensional Open System Apr 2001

NIFS-694 L N Vyacheslavov, K Tanaka, K Kawahata,
CO2 Laser Diagnostics for Measurements of the Plasma Density Profile and Plasma Density Fluctuations on LHD Apr 2001

NIFS-695 T Ohkawa,
Spin Dependent Transport in Magnetically Confined Plasma May 2001

NIFS-696 M Yokoyama, K Ida, H Sanuki, K Itoh, K Narihara, K Tanaka, K Kawahata, N Ohyabu and LHD experimental group
Analysis of Radial Electric Field in LHD towards Improved Confinement May 2001

NIFS-697 M Yokoyama, K Itoh, S Okamura, K Matsuoka, S -I Itoh,
Maximum-J Capability in a Quasi-Axisymmetric Stellarator May 2001

NIFS-698 S-I Itoh and K Itoh,
Transition in Multiple-scale-lengths Turbulence in Plasmas May 2001

NIFS-699 K Ohi, H Naitou, Y. Tauchi, O Fukumasa,
Bifurcation in Asymmetric Plasma Divided by a Magnetic Filter May 2001

NIFS-700 H Miura, T Hayashi and T Sato,
Nonlinear Simulation of Resistive Ballooning Modes in Large Helical Device June 2001

NIFS-701 G Kawahara and S Kida
A Periodic Motion Embedded in Plane Couette Turbulence June 2001

NIFS-702 K Ohkubo,
Hybrid Modes in a Square Corrugated Waveguide June 2001

NIFS-703 S -I Itoh and K Itoh,
Statistical Theory and Transition in Multiple-scale-lengths Turbulence in Plasmas June 2001

NIFS-704 S Toda and K Itoh,
Theoretical Study of Structure of Electric Field in Helical Toroidal Plasmas June 2001

NIFS-705 K. Itoh and S-I Itoh,
Geometry Changes Transient Transport in Plasmas June 2001

NIFS-706 M Tanaka and A Yu Grosberg
Electrophoresis of Charge Inverted Macroion Complex Molecular Dynamics Study July 2001

NIFS-707 T-H Watanave, H Sugama and T Sato
A Nondissipative Simulation Method for the Drift Kinetic Equation July 2001

NIFS-708 N Ishihara and S Kida,
Dynamo Mechanism in a Rotating Spherical Shell: Competition between Magnetic Field and Convection Vortices July 2001

NIFS-709 LHD Experimental Group,
Contributions to 28th European Physical Society Conference on Controlled Fusion and Plasma Physics (Madeira Tecnopolo, Funchal, Portugal, 18-22 June 2001) from LHD Experiment July 2001

NIFS-710 V Yu Sergeev, R K Janev, M J Rakovic, S Zou, N Tamura, K V Khlopenkov and S Sudo
Optimization of the Visible CXRS Measurements of TESPEL Diagnostics in LHD; Aug 2001

NIFS-711 M. Bacal, M Nishiura, M Sasao, M. Wada, M Hamabe, H Yamaoka,
Effect of Argon Additive in Negative Hydrogen Ion Sources, Aug 2001

NIFS-712 K Saito, R Kumazawa, T Mutoh, T Seki, T Watari, T Yamamoto, Y Torii, N Takeuchi C Zhang, Y Zhao, A. Fukuyama, F Shimpo, G. Nomura, M Yokota, A Kato, M Sasao, M. Isobe, A V Krasilnikov, T Ozaki, M Osakabe, K Narihara, Y. Nagayama, S. Inagaki, K. Itoh, T Ido, S Morita, K Ohkubo, M Sato, S Kubo, T Shimozuma, H. Idei, Y Yoshimura, T Notake, O Kaneko, Y Takeiri, Y Oka, K Tsumori, K Ikeda, A. Komori, H Yamada, H Funaba, K Y Watanabe, S Sakakibara, R Sakamoto, J Miyazawa, K Tanaka, B J Peterson, N Ashikawa, S. Murakami, T Minami, M. Shoji, S Ohdachi, S Yamamoto, H Suzuki, K Kawahata, M Emoto, H Nakanishi, N Inoue, N Ohyabu, Y Nakamura, S Masuzaki, S Muto, K Sato, T Morisaki, M Yokoyama, T Watanabe, M Goto, I. Yamada, K Ida, T Tokuzawa, N Noda, K Toi, S. Yamaguchi, K Akaishi, A Sagara, K. Nishimura, K Yamazaki, S. Sudo, Y. Hamada, O Motojima, M. Fujiwara,
A Study of High-Energy Ions Produced by ICRF Heating in LHD Sep 2001

NIFS-713 Y Matsumoto, S -I Ohkawa and T Watanabe,
Field Line and Particle Orbit Analysis in the Periphery of the Large Helical Device, Sep 2001

NIFS-714 S Toda, M Kawasaki, N Kasuya, K. Itoh, Y Takase, A Furuya, M Yagi and S -I Itoh,
Contributions to the 8th IAEA Technical Committee Meeting on H-Mode Physics and Transport Barriers (5-7 September 2001, Toki, Japan) Oct 2001